Optically Aligned, Space Resolving, Extreme Ultra-Violet and Soft X-ray Spectrograph

Michel Busquet[1], Frederic Thais[2], Ghita Geoffroy[2,3], Didier Raffestin[4] & J. P. Chièze[5]

[1] ARTEP, Inc., Ellicott City, MD, USA

[2] CEA/DSM/IRAMIS/SPAM, 91191 Gif-sur-Yvette Cedex, France

[3] CELIA, Université Bordeaux 1 & CEA & CNRS, Talence, France

[4] CEA/DAM/CESTA/Département des Lasers de Puissance, Centre d'Études Scientifiques et Techniques d'Aquitaine, BP 2, Le Barp Cedex, France

[5] Laboratoire AIM, IRFU/Service d'Astrophysique - CEA/DSM - CNRS - Université Paris Diderot, Bât. 709, CEA-Saclay, Gif-sur-Yvette Cedex, France

Correspondence: Michel Busquet, ARTEP, Inc., Ellicott City, MD, USA. E-mail: busquet@artepinc.com

Abstract

We describe in this paper an extreme ultra-violet/soft X-ray (XUV) spectrograph with high sensitivity, high spectral resolution and spatial resolution, which we developed to record XUV emission from a 10 J laser-irradiated gas jet. This spectrograph uses a flat field grazing incidence grating and a grazing incidence collection and imaging mirror. We designed a system where initial positions of elements can be set with a low accuracy of half a millimeter and where the final alignment is done with a visible light low intensity laser beam. High spectral resolution, good spatial resolution and nominal dispersion function have been achieved. A few illustrative results are presented.

Keywords: XUV spectrograph, spatial resolution, Xenon, gas jet, laser created plasma

1. Introduction

In extreme ultraviolet/soft X-ray (XUV, in the Astrophysics community the acronym EUV-X is also often used) spectral range (typically 1–30 nm), a high-resolution spectrograph ($\lambda / \Delta\lambda > 200$) is often sought. Up to now, transmission grating spectrographs have still moderate spectral resolution (~100 or less). And a high-resolution broadband XUV spectrograph requires grazing incidence optics, despite major advances in the fabrication of multilayer coatings which have still a restricted spectral range and a high cost. Moderate sensitivity of such spectrograph, or need for some spatial resolution, pushes to add a collection or imaging mirror, refocusing X-rays from the source. This mirror also operates with grazing incidence, allowing for high reflexivity.

In old days, it was not infrequent to spend weeks setting up XUV spectrograph equipped with grazing incidence grating. All components, entrance slit, grating and detector have to be precisely positioned on the Rowland circle–tangent to the grating and with a diameter equal to the radius of curvature of the grating (Rowland, 2012)–as the depth of field of this optical system is very narrow. Schwob and Fraenkel (Schwob, 1987, 1988; Filler, 1977) have even built a setup system based on a movable arm Michelson interferometer that allows speeding up the process. Nowadays, with a "flat field" grating (resulting from a non even spacing of the "groves" of the grating), the positioning accuracy is much less stringent as the depth of field is much larger. With the new XUV spectrograph we have designed and that we described in this paper, we go even further by using a low intensity-visible light He-Ne laser to setup and align the spectrograph. Although He-Ne laser are frequently used to align XUV light beam, to our knowledge, it has not been used for the setup of an XUV spectrograph. In addition, high sensitivity and spatial resolution are obtained by use of a toroïdal mirror that is also aligned with the same He-Ne laser beam. With our system, assembling, setup, fine tuning and alignment have been done in half a day. Design of our spectrograph is described in Section 2, setup and alignment process are described in Section 3. It allows a spectral resolution $\lambda/\Delta\lambda > 300$ and a spatial resolution of a few microns. Its sensitivity allows to record XUV spectrum of a few mJ of X-rays. Because settings start from the 0-th order beam, the computed and achieved wavelength dispersions are identical as shown in Section 4.

The XUV source we want to analyze is a 5–30 J laser irradiated Argon or Xenon gas jet, (Fiedorowicz, 1993, Doron, 1999) with segmented reflector in order to access the XUV albedo of various materials. We estimate the total energy in the XUV rays to be l J or less in the 4π. Some results obtained from this gas jet are presented in Section 5.

2. Description of the Apparatus

The schematic layout of our XUV spectrograph is presented in Figure 1. It is composed of 4 optical components: a collecting and imaging mirror "M", the entrance slit "S", the flat field grazing incidence grating "G" and the recording CCD camera. In addition there are 3 light shields "B_M", "B_S" and "B_G", blocking stray light and direct light from the X-ray emitting source and an additional light shield tunnel, not shown in Figure 1, around the light path from the entrance slit to the CCD camera. The grating "G" and the entrance slit are attached to a small table "T". This table stands on 3 feet of adjustable height that allow the table to be set "horizontal", i.e. parallel to the alignment He-Ne laser beam. Fine tuning of the table position will be described in the next section. The grating is set into a notch of this table, machined to the working incidence angle on the grating. In other words, the 0-th order is to be set parallel to the surface of table "T". We use in our experiment a gold coated, 1200±5 groves/mm (at center) flat field grating with a working angle of incidence of $\theta_i = 3°$. The height of the entrance slit above the table will be fine tuned with a vertical stage mechanical actuator. Everything, from the plasma to the CCD camera, is enclosed in one vacuum vessel pumped down to $P < 10^{-2}$ Pa (10^{-4} mbar).

For now on, we refer to distance along the "horizontal" axis as "z", the vertical axis is named "h" and the sagittal axis, i.e. perpendicularl to the tangential plane (z, h) is named "y". In this optical setup, the tangential plane is sometimes also called the meridional plane.

The mirror "M" is attached to a vertical translation stage (in the h direction) and to a rotation stage (with axis parallel to y) to be used during the final fine tuning. It is positioned at a horizontal distance d_{SM} (resp. d_{MP}) from the entrance slit (resp. from the X-ray source). The height H_C of the CCD can be changed to explore various spectral ranges. The "horizontal" distance from the grating to the entrance slit (resp. to the CCD imaging plane) is mechanically adjusted to the nominal value d_{GS} (resp. d_{CG}). These latter distances are given by the optical properties of the grating, as given by the manufacturer, though it has a depth of field large enough that it does not require high accuracy positioning. We achieved a better than 0.5 mm accuracy positioning which has been found to be enough in regard of the resolution we obtained (Section 4). The angle of incidence $\theta_i = 3°$ is precisely adjusted (see Section 3). The mirror "M" is a toroïdal mirror designed to give a tangential image of the plasma on the entrance slit and a sagittal image (i.e. image of the plasma in the y direction) on the CCD plane. In addition to the imaging capability in the y direction, it increases dramatically the collection angle, thus the sensitivity of the spectrograph. This high sensitivity would allow a 5 μm wide slit, but we ended with a 45 μm slit.

The incidence angle θ_M on the mirror is designed to be 6°. Let us call θ_0 the central reflection angle on grating (~10°). With Rz and R_Y the tangential radius and the sagittal radius, the focal lengths are respectively $f_Z = R_Z / 2 \, \sin\theta_M$ and $f_Y = R_Y / 2 \, \sin\theta_M$, thus the relations between the various distances read

$$\frac{1}{GM + GC} + \frac{1}{MP} = \frac{1}{f_Y} = \frac{2\sin\theta_M}{R_Y}$$

in the sagittal plane and

$$\frac{1}{SM} + \frac{1}{MP} = \frac{1}{f_Z} = \frac{2}{R_Z \sin\theta_M}$$

in the tangential plane.

Expanding distances GM, GC, SM and MP, it reads

$$\frac{1}{(d_{GS} + d_{SM})/\cos 2\theta_i + d_{CG}/\cos(\theta_o - \theta_i)} + \frac{\cos(2\theta_M - 2\theta_i)}{d_{MP}} = \frac{2\sin\theta_M}{R_Z}$$

$$\frac{\cos 2\theta_i}{d_{SM}} + \frac{\cos\left(2\theta_M - 2\theta_i\right)}{d_{MP}} = \frac{2}{R_Y \sin\theta_M}$$

The magnifying ratio γ (in the sagittal direction y) is simply given by the ratio of distances

$$\gamma = (d_{CG} + d_{GS} + d_{SM})/d_{MP}.$$

These distances are set to $d_{CG} = d_{GS} = 23.4$ cm, $d_{MP} = 21$ cm. The magnifying ratio is then ~3 and the mirror radii are equal to 2.02 m and 33.76 mm. These nominal values have been manufactured by the vendor with an accuracy of 1% on major radius and 0.1% on minor radius.
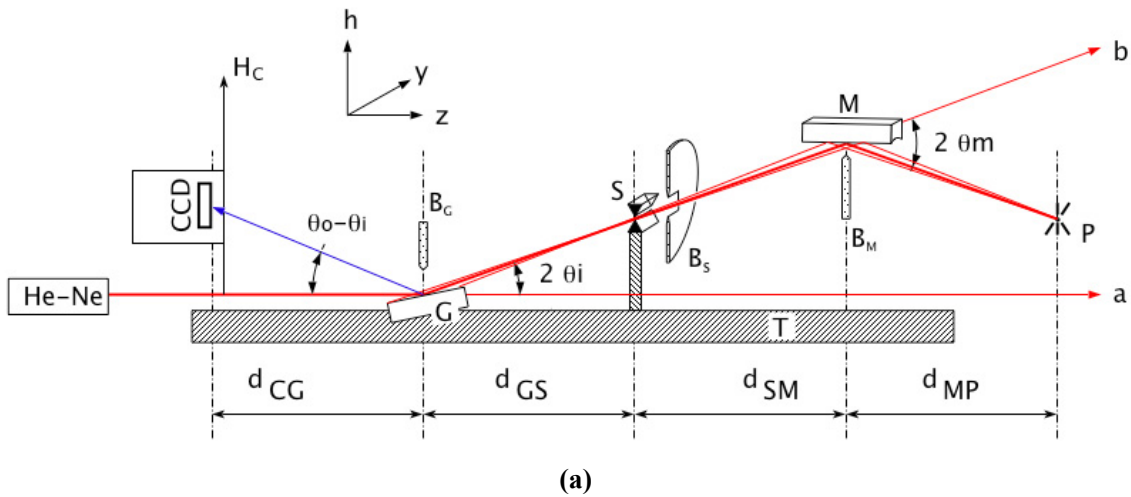

(a)

(b)
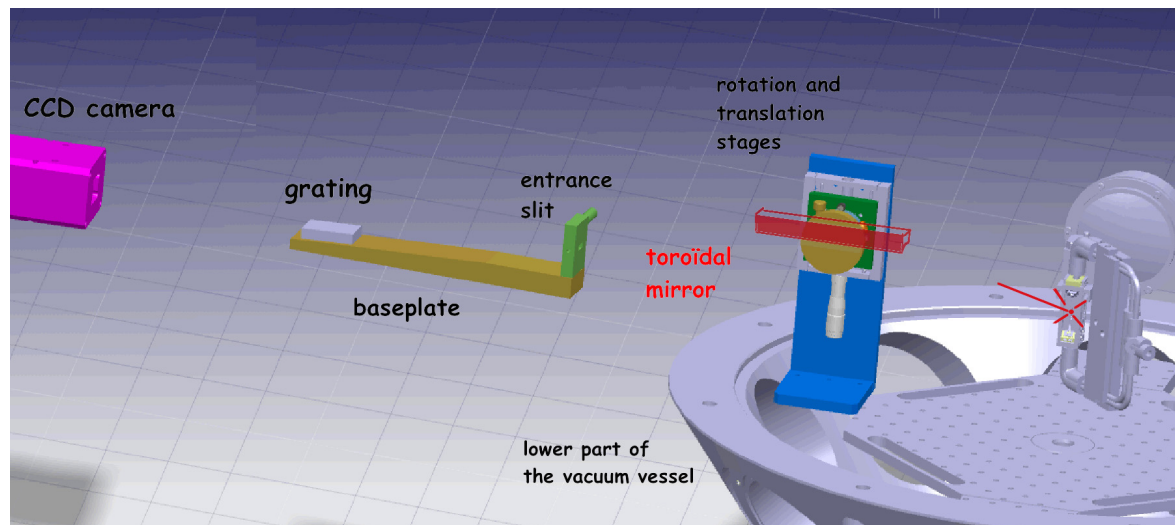
Figure 1. Spectrograph layout (a) and simplified CAD view (b) shows location of CCD, grazing incidence flat field grating (G), entrance slit (S), collection and imaging mirror (M), laser created plasma XUV source (P) and He-Ne alignment laser. The spectrograph table (T) can be adjusted "horizontal" (see definition in text). "a" (resp. "b") are the direction of the He-Ne laser beam when the grating G (resp. the mirror M) is set apart. A set of blocks (B_M, B_S, B_C, made of polyethylene) shields the stray light and allows only the intended light path. θ_M and θ_i are the incidence angles on mirror and grating, and θ_0 is the central reflection angle on grating. Fine tunings include the height of S and M, and the incidence angle on M

The CCD camera we used incorporates a back-illuminated 1340×1300 CCD without AR coating for ultra-low-energy X-ray detection. With 20×20 μm pixels and 100% fill factor, this system offers a large imaging area with very high spatial resolution and dynamic range. The thermoelectrically cooled design features Peltier

modules and electronic cards thermally linked to a circulating coolant (water) to provide reliable operation inside vacuum chambers. Note that with incomplete cooling, defaults of the CCD chip appear on image (as seen in Figure 3).

The computation of the dispersion function is straightforward. With θ_i and θ being the incidence and reflection angles, n being the order of reflection and λ the recorded wavelength, one get with a 1200 gr/mm grating

$$(\cos\theta - \cos\theta_i) * 10^7\text{Å} / 1200 = n\,\lambda$$

$$H = H_R + d_{GC} * \tan(\theta\text{-}3°)$$

where H_R is the reference height.

The dispersion functions obtained with these values are plotted in Figure 2 (eV or Å versus vertical position) were each set of 3 curves correspond

- to the nominal values of the angles and distances;

- and to values changed by adding the estimated uncertainty of $\pm\,0.1°$ on angles, and $\pm\,0.5$ mm on distances.

The reader interested in the spot diagram of such a combination of a flat field grating and an imaging toroïdal mirror would refer to (Choi, 1997).
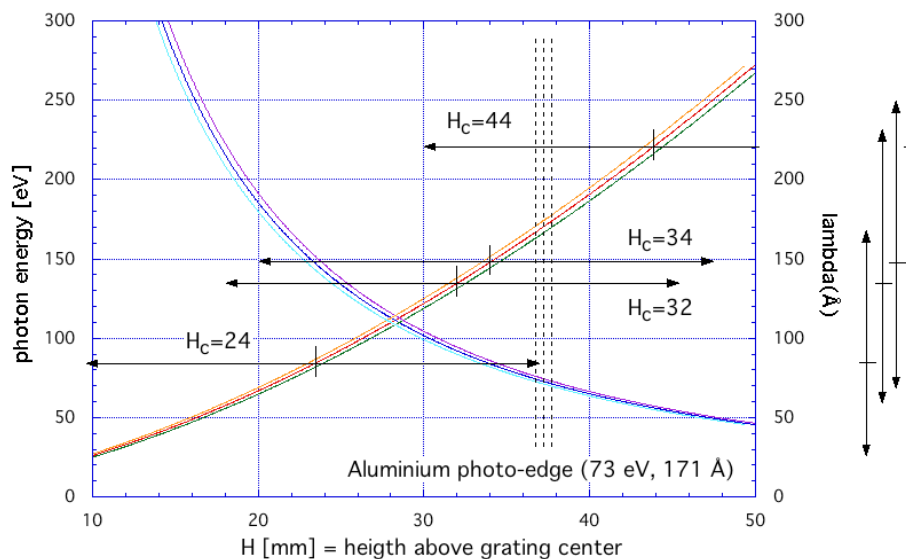

Figure 2. Theoretical dispersion functions accounting for uncertainty in the setting parameters. The 4 spectral ranges are identified by arrows, and are set by varying the height of the reading camera (Hc). The spectral ranges we used are indicated by arrows (in height in figure and in wavelength on the right side)

3. Fine Tuning and Alignment

The alignment and fine tuning proceed in 4 steps, all done in visible light from a standard red He-Ne laser.

We first set the He-Ne laser beam, more or less horizontal, in the convenient direction of XUV analysis. In our case it goes to the center of the experiment chamber,(note 1) shifted vertically by the computed height above the XUV emitting plasma, perpendicularly to the main laser beam that heats the gas jet and creates the plasma to be analyzed. From this step on, this He-Ne beam will be our "horizontal" reference.

The second step is to adjust the incidence angle on grating to the nominal value (3° in our case). For this we measure the deviation between incident and reflected He-Ne beam, noted "a" and "b" in Figure 1. This is done with the entrance slit and the beam blocks set off the beam path. The desired accuracy is obtained by measuring the spot deviation at 1m from the grating and adjusting the positioning screws on the 3 feet of table "T".

The third step is to adjust the height of the entrance slit into the He-Ne beam for maximum of transmission. Once done, the setting of the incidence angle and positions of grating and slit is achieved. Very good agreement with the theoretical dispersion function has been found (see Section 3). The 0-th order is given, by construction, by the He-Ne beam. By reverse imaging of the slit using this laser beam, we can now adjust the mirror position and

angle so the image of the XUV emitting plasma will be on the slit.

The final step is adjusting the image of the slit on the source position. This is done by rotating the mirror after setting its height, which has been done by locating the impact 'I' of the He-Ne beam at the center of the mirror. Fine adjustment of the transverse imaging (y direction) could further be done by adjusting the vertical height of the mirror, as it will move the impact 'I' away form the center of the mirror and thus will slightly change the distances d_{SM} and d_{MP}.

4. Wavelength Calibration

Once the previous settings have been done, grating position, slit position and incidence angle are now to their correct values, and will be not modified anymore. Neither shall we move the CCD camera distance to the grating D_{CG} or the mirror position and angles. But we can move the CCD camera in vertical position (H_C) along the dispersion direction, to select the spectral range. Repositioning at the same height can be done within a fraction of millimeter, to be compared to the geometrical size of the CCD of 26 mm.

We performed a few wavelength calibration shots (Figures 3–4), taking benefit of the cold Aluminium photo-edge at 170.5 Å (72.7eV) of a 0.2 μm Al filter and then using Oxygen lines from laser irradiated solid film of either plastic (C+H+O+N) or alumina (Al_2O_3). The wavelength of the Oxygen lines has been taken from the commercial description of an EUV lamp. (AIXUV, 2011) Position of the Al photo-edge, as well as the position of the Oxygen lines, has been found 0.5 mm higher than positions deduced from the measured height of the table T and of the camera holder above the spectrograph baseplate.
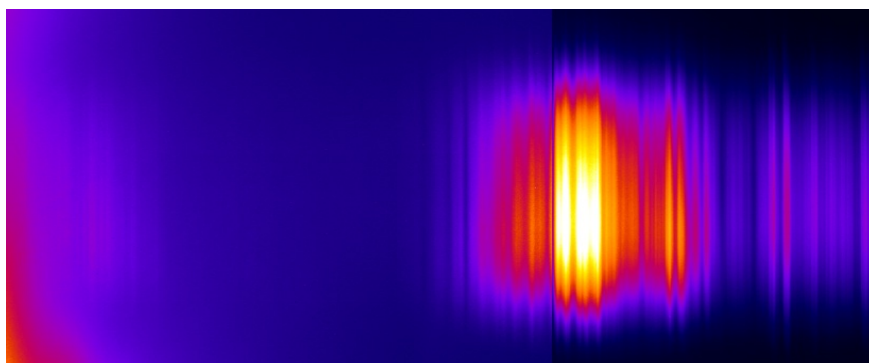
(a)
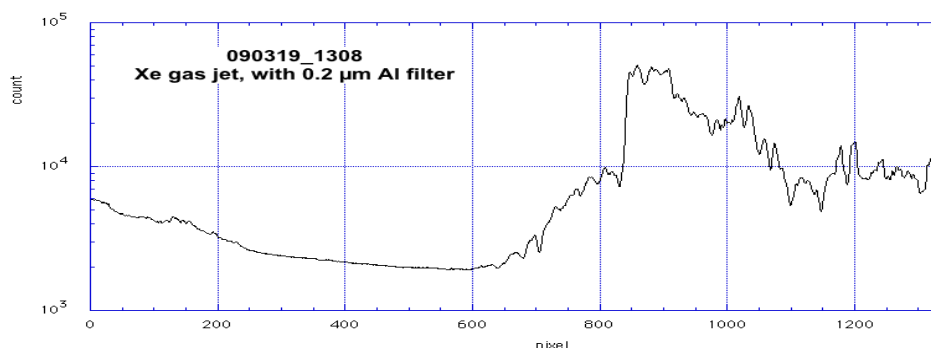
(b)

Figure 3. spatially resolved spectrum from hot Xe gas, filtered with 0.2 μm Al. (a) False colors (with a different color scale for pixel < 840), (b) lineout at center, note the cold Xenon absorption lines. Camera center height is set at 33.5±0.5 mm above grating center
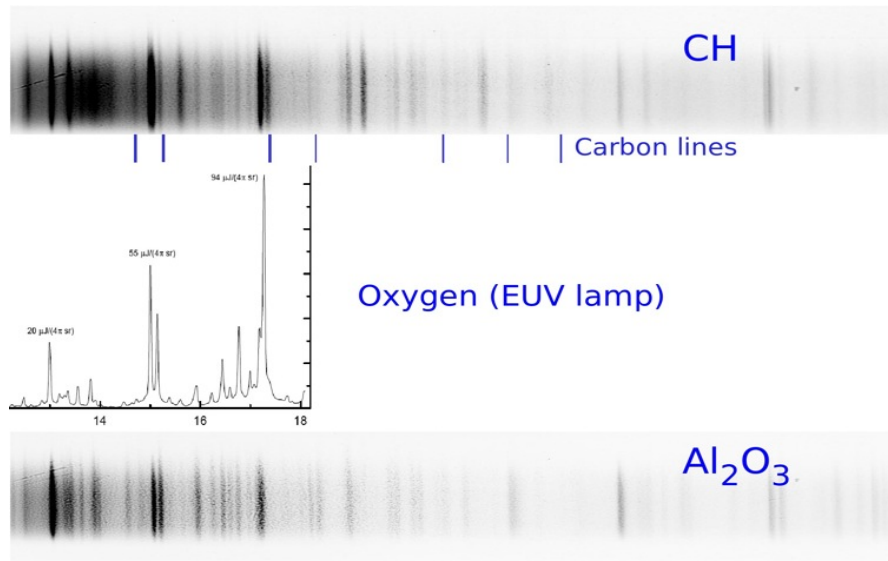
Figure 4. spectra from laser irradiated CH (top) and Al_2O_3 (bottom) solid target compared to a spectrum from an Oxygen EUV lamp (AIXUV 2011) This confirms the 12-34 nm theoretical wavelength range. Position of carbon lines is indicated. Grain and "scratches" come from incomplete cooling of the CCD

5. Results Obtained with a Laser Irradiated Xenon Jet

In this section, we illustrate spectral and spatial resolution obtained with this XUV spectrograph. Analysis of the involved physics will be presented elsewhere. The XUV source we analyze is a laser created plasma obtained with a 5-20 J, 3 ns, 10^{14} W/cm^2 laser pulse shining an Argon or Xenon gas jet. In some shots, a segmented sample of various compositions is placed behind the jet and re-emits part of the emitted XUV towards the spectrograph. Figure 5 presents a high energy Xenon spectrum (70–400 eV or 30–175 Å) obtained with a low energy shot (10 J). Although saturated in some place (white zones), this record illustrates the achieved high spectral resolution and spatial resolution. Absorption lines from surrounding colder Xenon can be seen. Below 50Å (225 eV), blooming from the 0-th order prevents any reading. Note that saturation leads to depleted pixels (below the white zones in Figure 5) as usual from CCD cameras. However we used a "large" entrance slit (45 μm) in the shots presented here, and we probably could go to a 5 μm wide slit. The spectral resolution is limited by the size of the pixels (1/1340 the recorded spectral range) which converts into $\Delta\lambda \sim 0.2$ Å at the center of the window. Using the 45 μm slit we demonstrated (Figure 5) a resolution better than 0.5 Å ($\lambda/\Delta\lambda > 300$). Going to a higher resolution is possible but would require either a smaller spectral range or an expansive 2500 pixels wide camera.
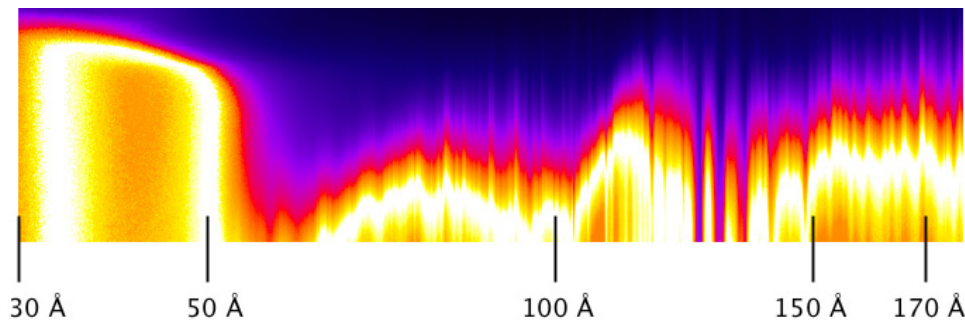

Figure 5. A 30-175 Å Xenon spectrum (obtained with a central height $H_C = 24$ mm) illustrates the achieved high resolution and the spatial resolution. Absorption bands from colder Xenon can be seen. Due the "large" slit width (45 μm) and "high" laser energy (15 J) used for this shot, saturation has been reached. Saturated pixels are displayed in white. Pixels below these are depleted and read with lower values. At wavelength below 50 Å, blooming from the 0-th order is observed

Segmented reflector of various materials was used to study reflective power (or albedo) of warm solid material, taking benefit of the spatial resolution. The reflection includes absorption of incident X-rays, heating of the material and re-emission with possibly a different spectrum. In Figure 6 the record evidences variation in albedo between heated Au (upper part of the image) and heated Al (lower part of the image). We estimate the temperature of the Xenon gas and of the reflector around 20–30 eV. Once again, one can note the high spectral resolution achieved, even with the wide entrance slit we used. We have not measured the spatial resolution, which should be below 20 microns.
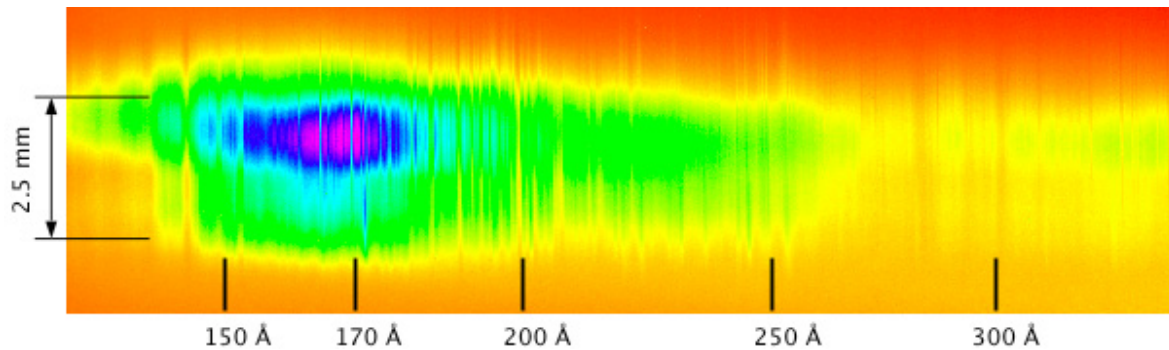

Figure 6. A 75-250 Å Xenon spectrum with segmented reflector (none-Au-Al from top to bottom) behind the gas jet

6. Conclusions

With sturdy mechanics and on-shelves components, we achieved a XUV spectrograph in the 50-350 Å range (35-250 eV) with high spectral resolution, high sensitivity and spatial resolution. It allows simple and easy setting and alignment, using a small He-Ne red laser, because we start from the 0-th order actual position. We align the spectrograph by moving the slit, not the grating, and precisely adjusting the collection/imaging mirror at the very end. This spectrograph can be assembled, set up and aligned in half a day. This new way of setup has permitted to obtain such achievements. Recorded spatially resolved spectra of high quality have been obtained.

Acknowledgments

References

AIXUV. (2011). Oxygen spectra with O V and O VI lines, as emitted from an EUV lamp. In *technical specs for the AI XUV's EUV-LAMPs*. Retrieved from http://www.aixuv.de/DOKUS/PRODUKTINFOS/AIXUV_LAMP_INFOS.pdf

Choi, I. W., Lee, J. U., & Nam, C. H. (1997). Space-resolving flat-field extreme ultraviolet spectrograph system and its aberration analysis with wave-front aberration. *Applied Optics, 36*(7), 1457. http://dx.doi.org/10.1364/AO.36.001457

Doron S., Behar, E., Mandelbaum, P., Schwob, J. L., Fiedorowicz, H., Bartnik, A., … Wilhein, T. (1999). Spectroscopic signature of strong dielectronic recombination in highly ionized xenon produced by irradiating a gas puff with laser. *Phys. Rev. A, 59*, 188. http://dx.doi.org/10.1103/PhysRevA.59.188

Fiedorowicz, H., Rymell, L., & Hertz, H. M. (1993). Droplet-target laser-plasma source for proximity X-ray lithography. *Appl. Phys. Lett., 62*, 2778. http://dx.doi.org/10.1063/1.116203

Filler, A., Schwob, J. L., & Fraenkel, B. S. (1977). Extreme grazing incidence spectrometer with interferometric adjustment for high resolution. In M. C. Caster, M. Pouey, & N. Pouey (Eds.), *Proceedings of the Fifth International Conference on the Vacuum Ultraviolet and Radiation Physics*, CNRS, Paris, 1977, Vol. III, pp. 86-88.

Rowland.   (2012).   X-ray   fluorescence.   Retrieved   September,   2012   from
    http://en.wikipedia.org/wiki/Rowland_circle#Monochromators

Schwob, J. L., Wouters, A. W., Suckewer, S., & Finkenthal, M. (1987). High-resolution duo-multichannel
    soft x-ray spectrometer for tokomak plasma diagnostics. *Rev. Sci. Instrum., 58*, 1601,
    http://dx.doi.org/10.1063/1.2818808

Schwob, J. L., Mexmain, J. M., Busquet, M., Bourgade, J. L., Louis-Jacquet, M., Demascureau, J., &
    Sauneuf, R. (1988). High-resolution multichannel XUV spectrometer with a 3-picosecond
    time-resolution for laser-produced plasmas diagnostics. *Journal de Physique, 49*(C1), 43-46,
    http://dx.doi.org/10.1051/physcol.1988106

Notes

Note 1: The center of the chamber is an arbitrary point, set once, to which laser beams, visualization
    tele-microscopes and other diagnostics are aligned to.